CANCER

Small-molecule targeted therapies induce dependence on DNA double-strand break repair in residual tumor cells

Moiez Ali[1], Min Lu[1], Hazel Xiaohui Ang[1], Ryan S. Soderquist[1], Christine E. Eyler[1], Haley M. Hutchinson[1], Carolyn Glass[2], Christopher F. Bassil[1], Omar M. Lopez[1], D. Lucas Kerr[3], Christina J. Falcon[4], Helena A. Yu[4], Aaron N. Hata[5], Collin M. Blakely[3], Caroline E. McCoach[3], Trever G. Bivona[3], Kris C. Wood[1]*

Residual cancer cells that survive drug treatments with targeted therapies act as a reservoir from which eventual resistant disease emerges. Although there is great interest in therapeutically targeting residual cells, efforts are hampered by our limited knowledge of the vulnerabilities existing in this cell state. Here, we report that diverse oncogene-targeted therapies, including inhibitors of epidermal growth factor receptor (EGFR), anaplastic lymphoma kinase (ALK), KRAS, and BRAF, induce DNA double-strand breaks and, consequently, ataxia-telangiectasia mutated (ATM)–dependent DNA repair in oncogene-matched residual tumor cells. This DNA damage response, observed in cell lines, mouse xenograft models, and human patients, is driven by a pathway involving the activation of caspases 3 and 7 and the downstream caspase-activated deoxyribonuclease (CAD). CAD is, in turn, activated through caspase-mediated degradation of its endogenous inhibitor, ICAD. In models of *EGFR* mutant non–small cell lung cancer (NSCLC), tumor cells that survive treatment with small-molecule EGFR-targeted therapies are thus synthetically dependent on ATM, and combined treatment with an ATM kinase inhibitor eradicates these cells in vivo. This led to more penetrant and durable responses in *EGFR* mutant NSCLC mouse xenograft models, including those derived from both established cell lines and patient tumors. Last, we found that rare patients with *EGFR* mutant NSCLC harboring co-occurring, loss-of-function mutations in *ATM* exhibit extended progression-free survival on first generation EGFR inhibitor therapy relative to patients with *EGFR* mutant NSCLC lacking deleterious *ATM* mutations. Together, these findings establish a rationale for the mechanism-based integration of ATM inhibitors alongside existing targeted therapies.

INTRODUCTION

Oncogene-targeted therapies have the potential to selectively eradicate tumor cells while sparing healthy tissues, a notion supported by evidence of remarkable activity in a subset of patients with cancer. For this reason, a number of targeted therapies, including epidermal growth factor receptor (EGFR) inhibitors in *EGFR* mutant non–small cell lung cancer (NSCLC), anaplastic lymphoma kinase (ALK) inhibitors in *ALK*-rearranged NSCLC, BRAF/MEK (mitogen-activated or extracellular signal–regulated protein kinase kinase) inhibitors in *BRAF* mutant melanomas, and tropomyosin receptor kinase (TRK) inhibitors in neurotrophic tyrosine receptor kinase (*NTRK*) fusion-positive tumors have become mainstays of clinical treatment, and many additional targeted therapies are now advancing through preclinical and clinical development (*1*–*3*). Unfortunately, it is also now well established that the depth and duration of responses to these agents are limited in patients with advanced disease, because most patients progress on the time scale of months. At that point, treatment options become limited, because many mechanisms of resistance are either unknown or cannot be pharmacologically targeted and patients often simultaneously harbor multiple distinct resistance mechanisms (*4*, *5*). This challenging reality underscores the importance of identifying more effective strategies to improve the upfront depth and duration of response to targeted therapies (*6*, *7*).

Extensive studies have examined the interplay between DNA-damaging chemotherapies or radiation therapy and resultant cellular DNA damage and repair processes. By contrast, we know relatively little about the impact of oncogene-targeted therapies on these processes. Three recent studies demonstrated that inhibitors of the EGFR/RAF/MEK/extracellular signal–regulated kinase (ERK) pathway cause transcriptional suppression of key genes involved in homologous recombination (HR) and mismatch repair (*8*–*10*). Similarly, another pair of recent studies showed that phosphatidylinositol 3-kinase (PI3K) inhibition can also suppress HR, potentially through a modulation of ERK activity (*11*, *12*). Thus, targeted therapy–induced suppression of DNA repair processes such as HR can lead to a "BRCA-like" state in cancer cells that sensitizes them to poly(adenosine diphosphate–ribose) polymerase (PARP) inhibitors or agents like histone deacetylase 3 inhibitors that can suppress expression of nonhomologous end joining genes (*8*, *9*, *11*, *12*). Supporting these observations, a recent phase 1 clinical trial indicated that the combination of the PI3Kα-specific inhibitor alpelisib and the PARP inhibitor olaparib yielded encouraging activity in patients with epithelial ovarian cancer (*13*).

Here, we report that targeted therapies induce DNA double-stranded breaks (DSBs) and consequent DSB repair in surviving cancer cells through a pathway involving the activation of executioner caspases 3 and 7 and the downstream endonuclease caspase-activated

[1]Department of Pharmacology and Cancer Biology and Duke Cancer Institute, Duke University, Durham, NC 27710, USA. [2]Department of Pathology, Duke University, Durham, NC 27710, USA. [3]Department of Medicine and Helen Diller Family Comprehensive Cancer Center, University of California, San Francisco, San Francisco, CA 94143, USA. [4]Thoracic Oncology Service, Division of Solid Tumor Oncology, Department of Medicine, Memorial Sloan Kettering Cancer Center, Weill Cornell Medical College, New York, NY 10065, USA. [5]Massachusetts General Hospital Cancer Center and Harvard Medical School, Charlestown, MA 02129, USA.
*Corresponding author. Email: kris.wood@duke.edu

deoxyribonuclease (CAD). Consequently, targeted therapy treatments create a synthetic dependence on the ataxia-telangiectasia mutated (ATM) kinase, a central coordinator of DSB repair. Combining oncogene-targeted therapies with ATM inhibitors thus eradicates residual tumor cells that would otherwise survive treatment, leading to more penetrant and durable therapeutic responses in cellular and animal models. Consistent with these observations, we find that, in patients with *EGFR* mutant NSCLC, ATM activation is observed in tumors treated with EGFR inhibitor therapy, and progression-free survival is extended when tumors harbor co-occurring *ATM* loss-of-function mutations. This work thus sets the stage for clinical studies investigating the integration of ATM inhibitors alongside existing targeted therapies.

RESULTS

DNA damage is observed in cancer cells surviving targeted therapy treatments

To examine whether treatment of oncogene-driven cancer cells with targeted therapies results in DNA damage and subsequent activation of DNA damage response (DDR) pathways, we began by using a panel of oncogene-driven cancer cell lines responsive to their cognate-targeted therapies. Treatment of *EGFR* mutant NSCLC, *ALK*-rearranged NSCLC, *KRAS* (Kirsten rat sarcoma viral oncogene homolog) mutant NSCLC, *BRAF* mutant melanoma, *FLT3* (fms-like tyrosine kinase 3) mutant acute myeloid leukemia (AML), and *KRAS* mutant pancreatic ductal adenocarcinoma cell lines with increasing doses of their cognate-targeted therapies for 24 hours led to increased amounts of autophosphorylated ATM at serine-1981 (S1981), a site required for activation of the downstream DDR pathway, and γ-H2AX, a canonical marker of DSBs [PC9, phosphorylated ATM (p-ATM), $P = 0.001$ and γ-H2AX, $P = 0.004$; A375, p-ATM, $P = 0.08$ and γ-H2AX, $P = 0.02$; HCC827, p-ATM, $P = 0.006$ and γ-H2AX, $P = 0.002$; MOLM13, p-ATM, $P = 0.06$ and γ-H2AX, $P = 0.05$; H3122, p-ATM, $P = 0.005$ and γ-H2AX, $P = 0.07$; and Mia PaCa-2, p-ATM, $P = 0.08$ and γ-H2AX, $P = 0.004$] (Fig. 1A and fig. S1A). To determine whether the observed DDR was a trivial consequence of drug-induced cell death, we treated a subset of these cell lines with low-dose targeted therapies and assessed cell viability following up to 7 days of drug exposure. At drug doses that did not affect cell viability, γ-H2AX induction was nevertheless observed (Fig. 1B and fig. S1B). Consistent with this result, we also observed gefitinib-induced increases in p-ATM and γ-H2AX in a panel of three independently derived gefitinib-resistant, *EGFR* mutant NSCLC cell lines whose growth was not affected by gefitinib treatment (p-ATM, $P = 0.09$ and γ-H2AX, $P = 0.08$) (Fig. 1C and fig. S1C). These gefitinib-resistant cell lines include PC9R, a pooled population of resistant cells derived by stepwise selection with gefitinib; PC9-WZR12, a clonally derived line with acquired resistance to both gefitinib and the third-generation irreversible EGFR inhibitor WZ4002 harboring both an $EGFR^{T790M}$ mutation and a *MAPK1* amplification; and PC9-GR4, harboring an $EGFR^{T790M}$ mutation (*14*). Consistent with these results, we observed no evidence of annexin V^+ staining in PC9 and A549 cells treated with cognate-targeted therapies at doses and a time scale on which a DDR is usually observed (Fig. 1D). Last, a neutral comet assay directly detected the presence of DSBs after a 24-hour targeted therapy treatment, as evidenced by an increased extent olive tail moment, suggesting that the observed ATM activation occurred because of DNA damage (Fig. 1E). Together, these data demonstrate that cancer cells surviving treatment with matched targeted therapies exhibit DNA DSBs and consequent ATM activation.

Targeted therapy treatment activates ATM kinase through mitochondrially stimulated caspase signaling

To better characterize the targeted therapy–induced DDR, we measured the activation state of ATM and ATR (ataxia telangiectasia and Rad3-related protein). ATM and ATR are members of the class IV PI3K-related kinase family of proteins, which serve as key regulators of the DDR, as well as downstream signaling pathways. Although no changes in ATR or phosphorylated Chk1 (S317), a marker of ATR activation, were seen in PC9 cells treated with gefitinib, phosphorylation of ATM and its substrate Chk2 (T68) were observed in two different EGFR inhibitor–sensitive cell lines (PC9 and HCC827; Fig. 2A and fig. S2A, respectively). In addition, similar activation of ATM and downstream effectors was observed in PC9 cells treated with the structurally distinct third-generation EGFR inhibitor osimertinib (fig. S2B). This effect was reversible (fig. S2C) and could be phenocopied via short hairpin RNA (shRNA)–mediated EGFR knockdown (fig. S2D). Because ATM appears to be the major DDR pathway activated after treatment with targeted therapies, we treated PC9 cells with AZD0156, a potent, selective, and orally bioavailable ATM inhibitor, alone or in combination with EGFR blockade. This treatment confirmed that combination of an ATM inhibitor and EGFR blockade abrogated both induction of γ-H2AX and activation of the DSB repair pathway (Fig. 2B). At higher doses of gefitinib, certain proteins involved in HR were down-regulated, such as exonuclease 1 (EXO1), BRCA1, and BRCA2, consistent with recently described findings (fig. S2E) (*10*). Together, these data demonstrate that EGFR inhibition leads to a DSB repair response coordinated by ATM.

During these studies, we noticed that treatment with increasing doses of gefitinib led to a dose- and time-dependent activation of ATM and γ-H2AX along with cleavage of both initiator caspase 9 and executioner caspase 3 (Fig. 2, C and D). A recent study demonstrated that activation of intrinsic pathway caspases can cause the formation of DSBs and subsequent activation of ATM, even when those caspases are activated at sublethal amounts (*15*). Thus, we hypothesized that caspase activation, occurring downstream of BIM and BAK/BAX activation and the resultant mitochondrial outer membrane permeabilization (MOMP) (Fig. 2D) (*16*), could be responsible for the observed DSB formation and ATM activation in cells surviving treatment with targeted therapies. Clustered regularly interspaced short palindromic repeats (CRISPR)–mediated knockout of BIM and RNA interference (RNAi)–mediated knockdown of BAX (but not BAK) abrogated targeted therapy induced ATM and γ-H2AX activation in PC9 cells (Fig. 2E and fig. S2, F and G), which is consistent with previous studies showing the preferential activation of BAX via BIM (*17*). To further test this hypothesis, we used the pan-caspase inhibitor Q-VD-OPh (quinoline-Val-Asp-difluorophenoxymethylketone), which was sufficient to abrogate the activation of ATM observed with EGFR inhibition alone (Fig. 2F). More specifically, our results point to the canonical executioner caspases 3 and 7 as drivers of the DDR, because CRISPR-Cas9–mediated knockout of both of these proteins at the same time abrogated both ATM activation and γ-H2AX formation in PC9 cells treated with gefitinib (Fig. 2G and fig. S2H), a mechanism that we also validated in an additional model of *EGFR* mutant NSCLC (fig. S2, H and I).

CAD is a key enzyme activated by caspases 3 and 7 that has previously been shown to mediate the formation of DSBs (*15*). Although

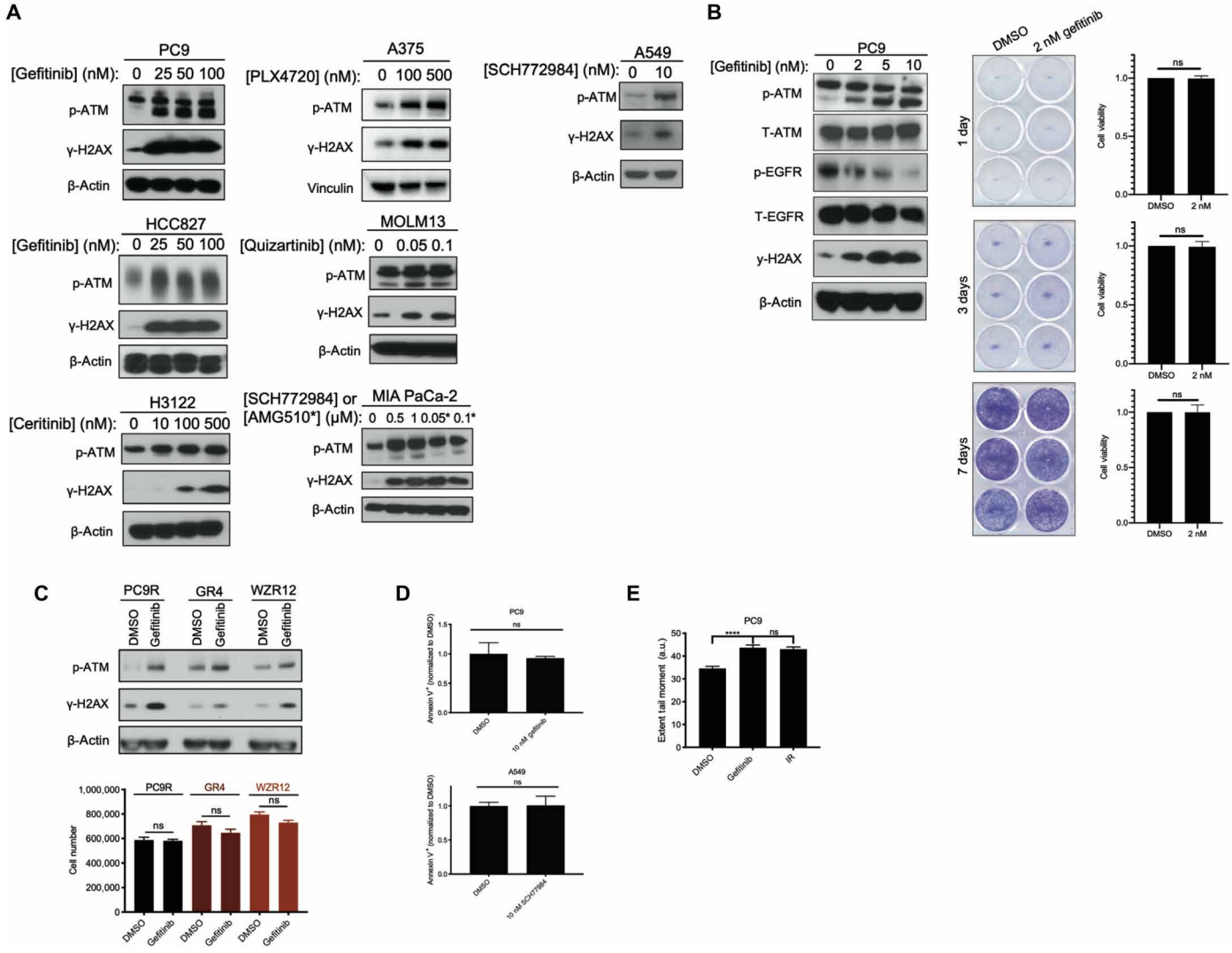

Fig. 1. DDRs in cells treated with targeted therapies. (**A**) Immunoblot of NSCLC, melanoma, AML, and pancreatic cancer cell lines after 24 hours of drug treatment with increasing concentrations of cognate-targeted therapies, probing for marks of DSBs, including p-ATM at S1981 and γ-H2AX. PC9 and HCC827 are *EGFR* mutant NSCLC, H3122 is *ALK*-rearranged NSCLC, A549 is *KRAS*(*G12S*) mutant NSCLC, A375 is *BRAF* mutant melanoma, MOLM13 is *FLT-3* mutant AML, and MIA PaCa-2 is *KRAS*(*G12C*) mutant pancreatic cancer. Gefitinib is an inhibitor of EGFR, ceritinib is an inhibitor of ALK, SCH772984 is an inhibitor of ERK1/2, PLX4720 is an inhibitor of BRAF, quizartinib is an inhibitor of FLT-3, and AMG510 is an inhibitor of KRAS(G12C). (**B**) Immunoblot of PC9 cells treated with the indicated doses of gefitinib for 24 hours, alongside cell viability measures as assessed by crystal violet staining of cells in clonogenic assay plates or Cell Titer Glo (CTG) after treatment with vehicle (DMSO) or gefitinib for the indicated periods of time. $N = 3$ for all cell viability experiments, where the mean ± SEM is plotted. *P* values were determined using unpaired, two-tailed Student's *t* tests. (**C**) Cell counts after 24 hours of 100 nM gefitinib drug exposure in drug-resistant NSCLC cells, alongside immunoblots of the corresponding drug-treated populations of cells. $N = 3$ for cell count experiments, where the mean ± SEM is plotted. *P* values were determined using unpaired, two-tailed Student's *t* tests. (**D**) Annexin V^+ staining (normalized to DMSO vehicle control) in drug-treated populations of NSCLC cell lines. $N = 3$ for the annexin V^+ staining experiments, where the mean ± SEM is plotted. *P* values were determined using unpaired, two-tailed Student's *t* tests. (**E**) Bar graph quantification of extent tail moment [arbitrary units (a.u.)] from neutral comet assay performed in PC9 cells after treatment with 100 nM gefitinib for 24 hours [ionizing radiation (IR) dose, 10 Gy]. $N = 503$ for DMSO treatment, $N = 704$ for gefitinib treatment, and $N = 645$ for IR treatment. The mean ± SEM is plotted. *P* values were determined using one-way ANOVA with Tukey's post hoc test. $^{****}P < 0.0001$; ns, not significant.

CAD expression was relatively unchanged after treatment of PC9 cells with gefitinib, expression of ICAD, an endogenous inhibitor of CAD that is directly cleaved by executioner caspases (*15*), was markedly reduced after treatment at the same doses ($P = 0.003$) (Fig. 2H and fig. S2B). This loss of ICAD was abrogated after CRISPR-Cas9–mediated knockout of caspases 3 and 7 (fig. S2J) and was due to a decreased half-life of the protein after targeted therapy treatment ($P = 0.03$). Consistent with caspase-mediated degradation, this coincided with increased amounts of active cleaved caspase 3 and active ATM (fig. S2K). Cleavage and degradation of ICAD is expected to result in CAD activation and consequent DSB formation and ATM activation. To test this model, we knocked out CAD using CRISPR-Cas9. In the absence of CAD, we no longer observed a targeted therapy–mediated induction of γ-H2AX expression or Rad51 foci, another marker of DSB repair, within PC9 cells (Fig. 2, I to L, and fig. S2L). The presence of CAD was also shown to be crucial for

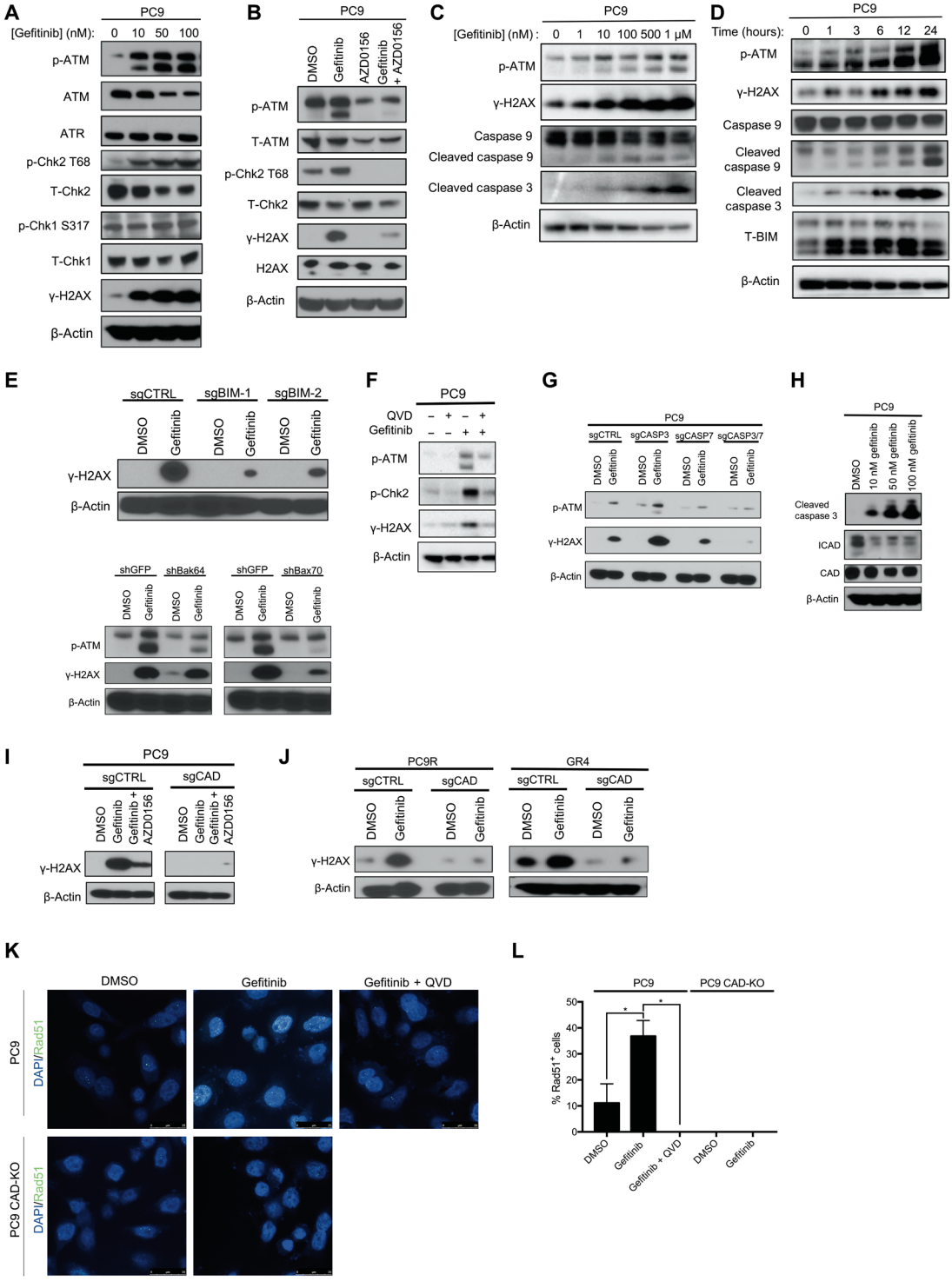

Fig. 2. Characterization of EGFR inhibitor–induced ATM pathway activation. (**A**) Immunoblotting of various DDR markers in PC9 cells after 24 hours of treatment with gefitinib at the indicated doses. (**B**) Immunoblot of PC9 cells after treatment with the EGFR inhibitor gefitinib (100 nM), AZD0156 (pharmacological inhibitor of ATM; 1.5 μM), or the combination of both EGFR inhibitor and ATM inhibitor (ATMi) for 24 hours. (**C**) Immunoblot of PC9 cells treated with increasing concentrations of gefitinib for 24 hours. (**D**) Immunoblot after treatment of PC9 cells with 100 nM gefitinib for the indicated lengths of time. (**E**) Immunoblot of 24-hour, 100 nM gefitinib-treated cells after CRISPR-Cas9–mediated knockout of BIM or RNAi-mediated short hairpin RNA (shRNA) knockdown of BAK/BAX in PC9 cells. (**F**) Immunoblot of PC9 cells treated with pan-caspase inhibitor Q-VD-OPh (2 μM), gefitinib (500 nM), or the combination for 24 hours. (**G**) Immunoblot of PC9 cells after CRISPR-Cas9–mediated knockout (KO) of caspase 3, caspase 7, or caspase 3 + caspase 7 after 24 hours of 100 nM gefitinib treatment. (**H**) Immunoblot of 24-hour, gefitinib-treated PC9 cells, revealing ICAD loss. (**I**) Immunoblot of 24-hour, 100 nM gefitinib-treated cells after CRISPR-Cas9–mediated knockdown of CAD in PC9 cells. (**J**) Immunoblot of the 24-hour, 100 nM gefitinib-treated cells after CRISPR-Cas9–mediated knockout of CAD in EGFR inhibitor–resistant cells. (**K**) Confocal microscopy images of Rad51 loading assay in PC9 cells after treatment with 100 nM gefitinib, Q-VD-OPh (2 μM), or the combination for 24 hours with and without the presence of CAD. DAPI, 4′,6-diamidino-2-phenylindole. (**L**) Bar graph quantification of images in (K). $N = 3$ for all groups presented, where the mean ± SEM is plotted. P values were determined using one-way ANOVA with Tukey's post hoc test. *$P < 0.05$.

DSB formation in two independently derived EGFR inhibitor–resistant populations (Fig. 2J and fig. S2L). Despite CAD knockout in PC9 cells, which resulted in abrogation of DDR activation after treatment with targeted therapy, we still observed cleavage of caspase 3 and loss of ICAD, underscoring the notion that caspase activation and ICAD loss effect function upstream of CAD activation (fig. S2M). In addition, CAD knockout reduced the drug-induced extent tail moment observed in the neutral comet assay to assess DNA DSBs in PC9 cells, supporting its proposed role in inducing the formation of DNA DSBs after targeted therapy treatment (fig. S2N). Last, consistent

with the hypothesis that ATM activity is required for the repair of targeted therapy–induced DNA damage, we observed increased Rad51 staining in cells treated with the EGFR inhibitor gefitinib and AZD0156 relative to vehicle or gefitinib alone (fig. S2, O and P).

Cancer cells surviving EGFR inhibitor therapy require ATM

The results above suggest that cells surviving treatment with targeted therapies may require ATM activity to resolve DSBs caused by targeted therapy exposure. This idea implies that ATM inhibition may have therapeutic value as a means of improving the depth and duration of responses to targeted therapies. To explore this hypothesis, we first treated cells with AZD0156, which blocked gefitinib-induced ATM activation (Fig. 2B). ATM inhibition sensitized EGFR inhibitor–sensitive and EGFR inhibitor–resistant cells to gefitinib, despite the fact that ATM inhibition was not associated with single-agent toxicity at these concentrations (Fig. 3A and fig. S3A). In addition, we confirmed that pharmacological inhibition of ATM conferred synergistic sensitization to EGFR inhibition in PC9 cells (combination index < 1.0 by Chou-Talalay method; table S1) (*18*). This effect was associated with combination therapy–induced increases in caspase 3 cleavage and annexin V staining (fig. S3, B and C), suggesting that increases in DSB formation caused by combined oncogene-targeted therapy and ATM inhibition results in cell death by apoptosis.

The notion that cells surviving EGFR inhibitor therapy are nevertheless sensitive to combined EGFR and ATM inhibition suggests that this combination strategy may be an effective means of ablating cells that survive upfront treatment with EGFR inhibitor monotherapy. To directly test this concept, PC9 cells were treated with an EGFR inhibitor dose 100-fold greater than the median inhibitory concentration (IC_{50}) of these cells (2 μM gefitinib or 1 μM osimertinib) for 9 days, selecting for a population of cells that are termed drug-tolerant persisters (DTPs) (*19*). Reflecting their exposure to EGFR inhibitor, DTP cells had higher expression of p-ATM compared to untreated, gefitinib-sensitive PC9 cells (fig. S3D). Consistent with our mechanistic studies, we observed the presence of cytochrome c in the cytoplasm of DTP cells, implying MOMP and caspase activation in these cells (fig. S3E). Furthermore, ATM inhibition sensitized these cells to EGFR blockade with gefitinib or osimertinib (Fig. 3B). Because resistance eventually emerges from cells that survive upfront drug treatments, we next hypothesized that combined EGFR and ATM inhibition may delay resistance evolution. In a long-term qualitative time-to-progression (TTP) assay (*20*), wherein cell population size is monitored over weeks during drug treatment to model the development of resistance in vitro, we observed that AZD0156 had only a minor effect on cell growth, and gefitinib monotherapy led to resistance outgrowth in around 40 days, whereas treatment with combined gefitinib and AZD0156 treatment effectively eradicated residual cells, leading to long-term suppression of resistance outgrowth (Fig. 3C). Similar results were seen after the use of the third-generation EGFR inhibitor, osimertinib, in EGFR inhibitor–sensitive and EGFR inhibitor–resistant populations of cells, both in short-term (3-day) experiments (Fig. 3D) and in a long-term (32-day) TTP assay (Fig. 3E). These long-term TTP findings were recapitulated in HCC827 cells (fig. S3F) and in two *KRAS* mutant cell lines treated with the ERK inhibitor SCH772984, expanding the application of the ATM inhibitor plus targeted therapy concept to non–EGFR-driven cell line models (fig. S3, F and G). Similar results were also observed in MGH119 cells, which were recently derived from a treatment-naïve patient with *EGFR* mutant NSCLC (*21*, *22*), with respect to EGFR inhibitor–induced γ-H2AX formation, ATM activation, and ATM inhibitor–mediated sensitization to EGFR blockade (Fig. 3F and fig. S3H). In addition, MGH119 DTPs showed a similar sensitization to the EGFR inhibitor gefitinib when treated in combination with AZD0156 (fig. S3I). ATM inhibitor–mediated sensitization to targeted therapy was only observed in cells treated with their cognate-targeted therapy as evidenced in a panel of *KRAS* mutant cell lines treated with gefitinib, to which these cell lines are relatively insensitive, or the ERK inhibitor SCH772984, to which they are sensitive (fig. S3, J and K). Last, having determined that DSB formation and ATM activation occur in a CAD-dependent manner after EGFR blockade, we assessed the impact of CAD on the cellular response to combined EGFR and ATM inhibition. CRISPR-Cas9–mediated CAD knockout rescued the toxicity of the dual therapy in short-term assays conducted in both EGFR inhibitor–sensitive and EGFR inhibitor–resistant cells (Fig. 3G). Similarly, in long-term TTP assays in PC9 cells, we observed that CAD knockout (sgCAD) led to the outgrowth of cells in the context of dual EGFR plus ATM inhibition, whereas cells expressing CAD (sgCTRL) were durably growth suppressed as expected (Fig. 3H). Last, we used RNAi technology to knock down the expression of ATM and found that loss of ATM abrogated gefitinib-induced γ-H2AX induction and phenocopied the ATM inhibitor AZD0156 in long-term TTP assays in PC9 cells, suggesting that AZD0156 functions in these contexts through on-target ATM inhibition (Fig. 3I and fig. S3L). Together, these results demonstrate that CAD-mediated formation of DSBs in cells surviving treatment with EGFR inhibitors imposes a synthetic dependence on ATM, a kinase critical for the resolution of this DNA damage. Thus, combined EGFR and ATM inhibition eradicates cell populations that otherwise survive EGFR inhibitor monotherapy, leading to long-term, CAD-dependent suppression of resistance outgrowth (Fig. 3J).

Pharmacological targeting of PARP sensitizes cells to EGFR inhibition

Having established that ATM inhibition can be used to effectively target cancer cells that survive EGFR inhibitor therapy, we sought to evaluate whether these findings could be extended to other DDR pathway inhibitors through a similar mechanism. Specifically, we focused on the PARP inhibitor olaparib, which is U.S. Food and Drug Administration–approved and indicated for use in multiple cancer contexts. After performing Western blots showing the effects of single-agent EGFR inhibitor (gefitinib) and PARP inhibitor (olaparib) treatment on PC9 cells (fig. S3M), we performed a similar panel of experiments to assess the effect of this combination on cell viability. The combination of EGFR plus PARP inhibition led to qualitatively similar but more modest effects than combined EGFR plus ATM inhibition in short-term assays performed in both parental PC9 cells and resistant derivatives treated with first- or third-generation EGFR inhibitors (fig. S3, N and O). In long-term TTP assays in PC9 cells, this combination mirrored more closely the effect of the EGFR plus ATM inhibitor combination (fig. S3P). Last, consistent with findings in combined EGFR plus ATM inhibitor–treated cells, CAD knockout rescued the viability of both EGFR inhibitor–sensitive and EGFR inhibitor–resistant cells treated with the combination of EGFR and PARP inhibitors (fig. S3Q). Thus, CAD-driven DNA damage in cells surviving treatment with EGFR inhibitors also creates a synthetic dependence on PARP.

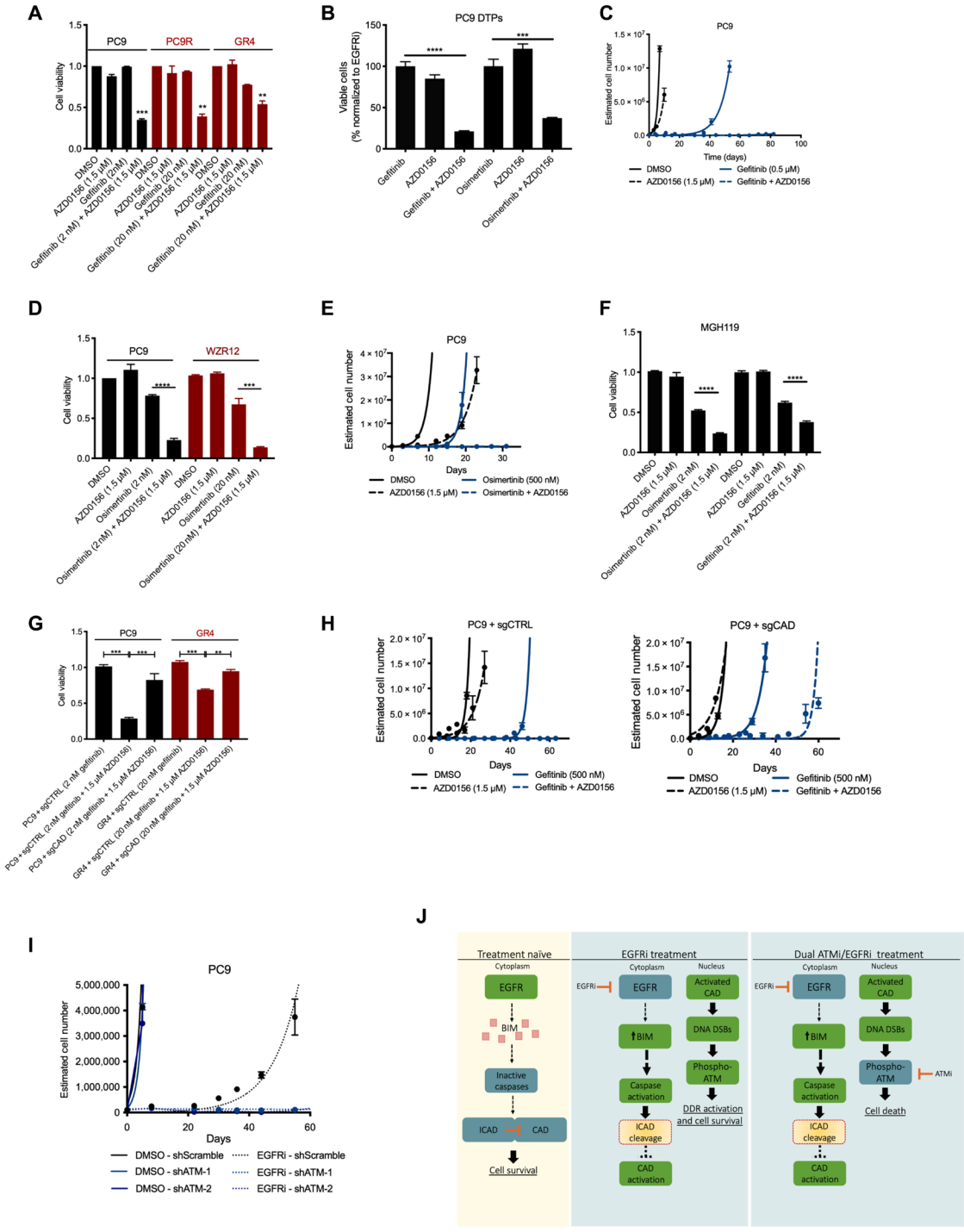

Fig. 3. Effect of ATM inhibition on survival and growth of EGFR inhibitor–resistant cells. (**A**) Cell viability in the indicated drug treatment conditions in EGFR inhibitor–sensitive (PC9) and EGFR inhibitor–resistant (PC9R and GR4) cells. (**B**) Cell viability, as assessed through the percentage of surviving cells (normalized to gefitinib-only treated), of PC9 drug-tolerant persisters (DTPs) after 4-day treatment with single-agent gefitinib (100 nM), AZD0156 (1.5 μM), or the combination. (**C**) Estimated cell number during long-term time-to-progression (TTP) assay of PC9 cells treated with gefitinib, AZD0156, or the combination. (**D**) Cell viability in the indicated drug treatment conditions in EGFR inhibitor–sensitive (PC9) and EGFR inhibitor–resistant (WZR12) cells. (**E**) Estimated cell number during long-term TTP assay of PC9 cells treated with osimertinib, AZD0156, or the combination. (**F**) Cell viability in the indicated drug treatment conditions in EGFR inhibitor–sensitive MGH119 cells. (**G**) Cell viability in the indicated drug treatment conditions in EGFR inhibitor–sensitive (PC9) and EGFR inhibitor–resistant (GR4) cells with or without CAD presence (sgCTRL or sgCAD, respectively). (**H**) Estimated cell number during long-term TTP assay of PC9 cells treated with gefitinib, AZD0156, or the combination, with or without CAD presence (sgCTRL or sgCAD, respectively). (**I**) Estimated cell number during long-term TTP assay of PC9 cells treated with vehicle or gefitinib, with or without ATM presence (shScramble or shATM, respectively). (**J**) Conceptual diagram linking EGFR inhibition to ATM activation and dependence. $N = 3$ for all cell viability assays and estimated cell number during long-term TTP assays presented, where the mean ± SEM is plotted. P values were determined using unpaired, two-tailed Student's t tests. $^{**}P < 0.01$; $^{***}P < 0.001$; $^{****}P < 0.0001$.

Combined inhibition of ATM and EGFR forestalls the outgrowth of tumors in vivo

To test the efficacy of the EGFR plus ATM inhibitor drug combination in vivo, we performed a xenograft study. Once subcutaneous PC9 tumors reached 100 to 200 mm^3, mice were randomized into one of four treatment arms including vehicle, single-agent EGFR inhibitor osimertinib, single-agent ATM inhibitor AZD0156, or the combination treatment. Whereas ATM inhibition alone had little effect on tumor growth, EGFR inhibitor monotherapy suppressed the growth of tumors before eventually giving rise to resistance outgrowth (Fig. 4, A and B). In contrast, mice treated with the combination of ATM and EGFR inhibitors displayed sustained tumor regressions that lasted throughout the length of the study. We observed no apparent toxicity based on body weight of the mice in this study (fig. S4A). On-target activity of the ATM and EGFR inhibitors and osimertinib-induced ATM activation were each verified via immunoblotting of mouse tumor lysates after treatment (fig. S4, B and C). These findings were confirmed in an additional *EGFR* mutant H1975 lung cancer xenograft model (Fig. 4, C and D, and fig. S4, D and E). Last, we used a panel of three cellular models recently derived from patients with lung cancer, which included MGH134 from a patient with *EGFR* mutant NSCLC who developed resistance to first-line erlotinib therapy via a $EGFR^{T790M}$ resistance mutation, MGH1109 from a treatment-naïve patient with *EGFR* mutant NSCLC, and MGH006 from a treatment-naïve patient with *EML4-ALK* variant 1 mutant NSCLC. We observed that ATM inhibition suppressed the outgrowth of resistance to matched targeted therapies in long-term TTP assays (fig. S4F). Consistent with this finding, osimertinib treatment yielded initial growth suppression followed by eventual tumor progression in MGH134 xenograft–bearing mice, whereas the combination of osimertinib plus AZD0156 yielded sustained tumor regressions that lasted throughout the length of the study (Fig. 4, E and F).

ATM activation is observed in tumors from patients treated with EGFR inhibitors

Last, to investigate potential clinical correlates of these findings, we first performed immunohistochemical (IHC) staining to quantify p-ATM S1981 expression in matched tumor samples taken from patients with *EGFR* mutant NSCLC before (treatment-naïve) and during (progressive disease) treatment with the EGFR inhibitor erlotinib. In five of the five cases, p-ATM staining was increased in tumors progressing on treatment with erlotinib relative to matched pretreatment tumor samples (Fig. 4, G and H). Aggregate analysis of all patient samples correspondingly revealed a significant increase in p-ATM expression in progressing tumors undergoing erlotinib treatment (Mann-Whitney test, $P = 0.0079$; Fig. 4I). Next, we hypothesized that rare patients with *EGFR* mutant NSCLC whose tumors harbor co-occurring loss-of-function mutations in *ATM* (<5% of patients) may exhibit more durable responses to EGFR kinase inhibitors than those whose *EGFR* mutant tumors lack loss-of-function *ATM* mutations. We queried the Memorial Sloan Kettering–Integrated Mutation Profiling of Actionable Cancer Targets (MSK-IMPACT) Clinical Sequencing Cohort database, which contained data on the time to clinical progression on first-line erlotinib therapy for 11 patients whose tumors contained co-occurring *EGFR* activating/erlotinib sensitizing mutations and *ATM* mutations (table S2). We annotated these *ATM* mutations as being either (1) likely loss-of-function/nonsense mutations or deleterious/damaging mutations (using the Sorting Intolerant From Tolerant (SIFT) and PolyPhen-2 tools), or (2) likely non-functional mutations. TTP on erlotinib in patients whose tumors harbor co-occurring loss-of-function *ATM* mutations was 17.8 ± 10.9 months compared to 9.0 ± 1.9 months in those patients whose tumors harbor likely nonfunctional *ATM* mutations ($P < 0.05$) (fig. S4G). Although the results of this analysis should be considered with care given the small sample size, we note that the latter figure is consistent with the time to clinical progression of 8 to 12 months observed in multiple studies of unselected patients with *EGFR* mutant NSCLC treated with first-line erlotinib therapy, including one study that used the same clinical cohort at the same institution (*23*). Together, these data suggest that ATM activation occurs in human tumors surviving treatment with EGFR inhibitors, where it likely plays a tumor-protective role. A summary of the key results of this study are summarized in the schematic shown in Fig. 4J.

DISCUSSION

The heterogeneous and multifocal nature of acquired resistance mechanisms to targeted therapies limits our ability to effectively treat and reverse resistance after it emerges (*4*–*7*). As a consequence, substantial efforts are now being expended to develop upfront treatment strategies capable of forestalling resistance evolution. To date, these strategies include upfront targeting of prevalent resistance mechanisms or points of convergent signaling downstream of key resistance mechanisms, identifying and targeting vulnerabilities unique to the DTP cells that survive initial treatment with oncogene-targeted therapies, and identifying and targeting "collateral sensitivities," which are scenarios where acquired resistance to an initial therapy produces heightened sensitivity to a second therapy (*4*–*7*, *24*–*30*). Here, we demonstrate that, by targeting ATM-dependent survival in cells undergoing treatment with targeted therapies, it is possible to increase the depth and duration of activity of those therapies. Because DNA damage induction may occur both in cells with preexisting resistance mechanisms and in DTP cells, we speculate that this approach may have advantages over strategies targeting only one of these two sources of resistance.

This work also fits into the broader context of targeting the DDR pathway as a cancer therapeutic strategy. The discovery that PARP inhibitors have specific activity in the context of *BRCA1/2* mutations led to the subsequent, successful deployment of PARP inhibitors for the treatment of certain *BRCA* mutant and HR-deficient tumors (*31*). This advance helped catalyze the development of additional agents targeting key nodes in the DDR network, including ATM, and the search for mutational contexts in which these drugs exhibit activity and mechanism-based combination therapies to enhance their activity (*31*). To date, however, many tumors lack mutations that confer sensitivity to these agents. Furthermore, most clinically advanced combination therapies involving these agents involve the use of DNA-damaging chemotherapies, inhibitors of other DDR pathway nodes, or modifiers of chromatin state, strategies that may cause increased toxicity to both tumor and normal cells (*31*). Clinical trials involving combinations of PARP inhibitors with chemotherapies like temozolomide, cisplatin, and gemcitabine have revealed exacerbated toxicity that required dose reductions, implying a narrow therapeutic index (*31*). Our present demonstration that oncogene-targeted therapies potentiate ATM inhibitor action through caspase activation, which has been shown to be specific to cells harboring sensitizing oncogenic driver mutations, is thus particularly promising, because it may enable tumor-selective activation of lethal DNA damage.

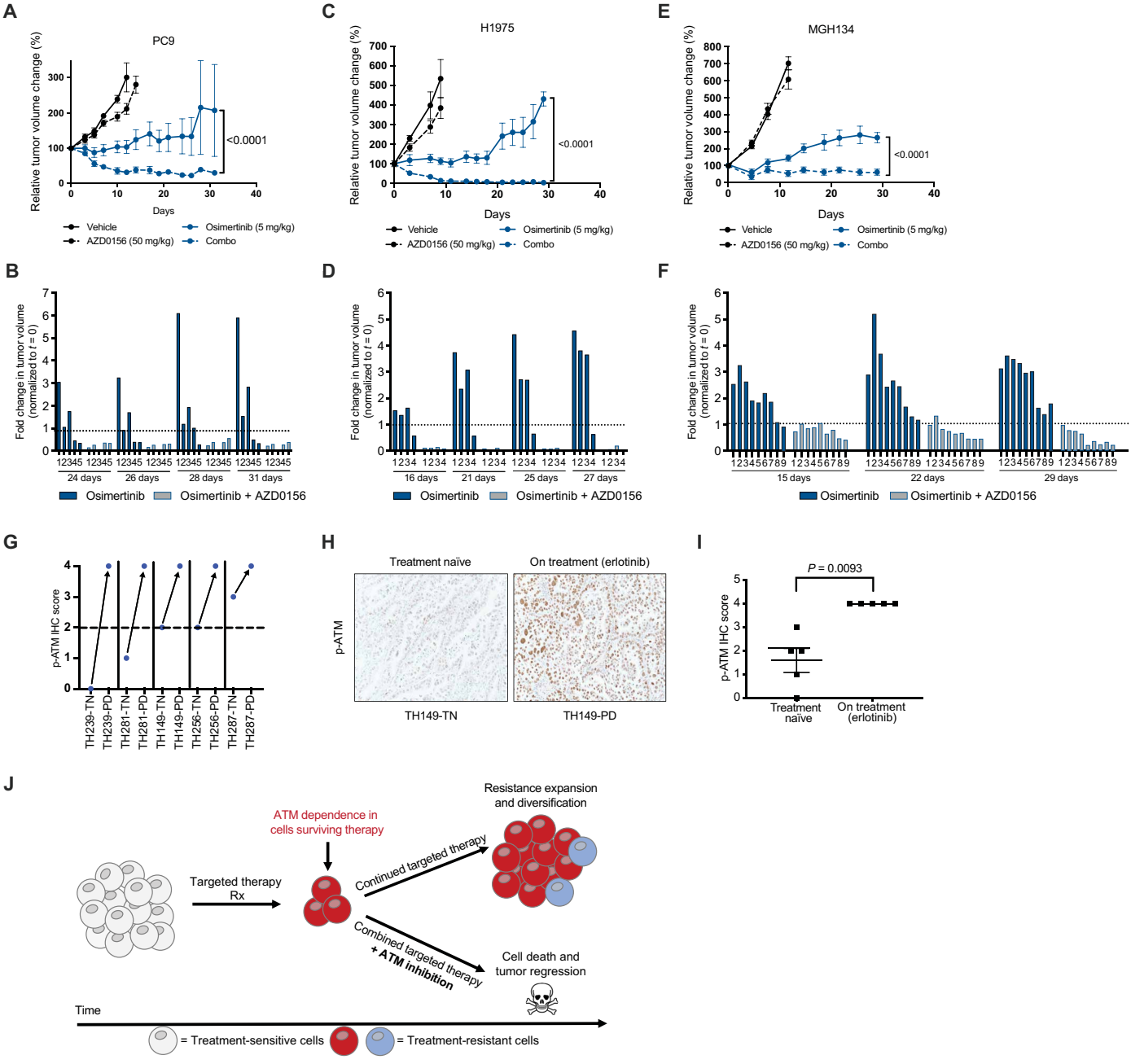

Fig. 4. Targeted therapy–induced ATM activation and targeting in vivo. (**A**) Tumor volume (normalized to $t = 0$, %) of PC9 cell line xenografts in nude mice after treatment with vehicle, osimertinib, AZD0156, or the combination for indicated time points ($n = 5$ mice in each treatment arm). *P* values were determined using unpaired, two-tailed Student's *t* test. (**B**) Fold change in individual tumor volume (normalized to $t = 0$) for PC9 tumors treated with osimertinib or the combination of osimertinib and AZD0156. (**C**) Tumor volume (normalized to $t = 0$, %) of H1975 cell line xenografts in nude mice after treatment with vehicle, osimertinib, AZD0156, or the combination for indicated time points ($n = 4$ to 5 mice in each treatment arm). *P* values were determined using unpaired, two-tailed Student's *t* tests. (**D**) Fold change in individual tumor volume (normalized to $t = 0$) for H1975 tumors treated with osimertinib or the combination of osimertinib and AZD0156. (**E**) Tumor volume (normalized to $t = 0$, %) of MGH134 patient-derived cell line xenografts in nude mice after treatment with vehicle, osimertinib, AZD0156, or the combination for indicated time points ($n = 9$ to 10 mice in each treatment arm). *P* values were determined using unpaired, two-tailed Student's *t* tests. (**F**) Fold change in individual tumor volume (normalized to $t = 0$) for MGH134 tumors treated with osimertinib or the combination of osimertinib and AZD0156. (**G**) p-ATM IHC score of patient tumor tissue obtained before [treatment naïve (TN)] or during treatment with erlotinib [progressive disease (PD)]. Same numbers indicate tumors longitudinally sampled from the same patient. (**H**) Representative image of p-ATM immunohistochemistry from patient tumors before treatment (TN) or during treatment (PD). Images taken at ×20 magnification. (**I**) p-ATM IHC scores from five matched tumor samples from patients with *EGFR* mutant lung adenocarcinoma taken at the time of diagnosis and at the time of relapse to EGFR inhibitor erlotinib. *P* values were determined using unpaired, two-tailed Student's *t* tests. (**J**) Proposed model of ATM dependence in targeted therapy–treated tumors, leading to rational combination of targeted therapies and ATM inhibitors.

Several open questions and potential limitations should be considered. First, although caspase activation is believed to be a common feature of tumor cells treated with oncogene-matched targeted therapies and we demonstrate targeted therapy–induced ATM activation in diverse oncogene-driven models, the full breadth of scenarios in which ATM inhibition may be used to potentiate the activity of targeted therapies is yet to be determined. Second, although our studies suggest that *TP53* mutational status does not influence cellular responses to combined EGFR and ATM inhibition (table S3), it remains to be determined whether other recurrent mutations, for example, in DDR pathway genes, influence responsiveness to these combination therapies. Last, a growing body of work suggests that DNA damage induction by PARP inhibitors may potentiate not only the toxicity of DNA-damaging chemo- and radiation therapies but also immune surveillance and checkpoint blockade. Thus, a key question for future studies is whether DNA damage secondary to combined targeted therapy plus ATM inhibition can potentiate inflammatory signaling, immune surveillance, and checkpoint inhibitor activity in tumors.

Together, the demonstration that ATM inhibition potentiates tumor responses to oncogene-targeted therapies is well positioned for near-term clinical development. Multiple selective ATM kinase inhibitors are currently in clinical development, including those with blood-brain barrier permeability (*32*), and preclinical studies suggest that these agents may have very favorable toxicity profiles. Thus, the studies presented here provide a clear, mechanism-based rationale for the near-term design of clinical trials in diverse malignancies currently treated with standard-of-care targeted therapy paradigms.

MATERIALS AND METHODS

Study design

The overall goal of this study was to determine the mechanism and translational implications of oncogene-targeted therapy–induced DNA damage. Specifically, this study focused primarily on EGFR inhibitor–targeted therapies in the context of *EGFR* mutant NSCLC and whether selective ATM inhibition could improve the depth and duration of response to these agents.

In vivo studies were performed using 6- to 8-week-old female nude mice. The number of mice used in each experimental group was determined on the basis of statistical power analysis to render statistical significance of the experimental data between different experimental groups and ranged from five to six mice per group. Before treatment, mice were randomized on the basis of tumor volume to ensure evenly distributed average tumor sizes across each group. Mouse survival end points were based on the maximum tumor volume allowed under the approved animal use protocol (1000 mm^3). Investigators received measurements of tumors with each treatment group and so were blinded from the actual treatment of mice in each group. Tumors that did not take (no viable tumors formed) were excluded from the study. All mouse studies were performed under protocols approved by the Institutional Animal Care and Use Committee and the Institutional Review Board of Duke University School of Medicine. The mice were housed in an animal facility that is free of specific pathogens. All mice were fed standard normal chow diet and housed under controlled temperature and 12-hour light/12-hour dark cycle conditions. The mice were under the general supervision of experienced veterinarians and were attended and monitored at least daily by a trained animal care technician.

Cell lines and reagents

All cell lines were maintained in a humidified incubator at 37°C with 5% CO_2. PC9, HCC827, H3122, A549, A375, GR4, WZR12, PC9R, MGH134, MGH006, MGH1109, and MOLM13 were cultured in RPMI 1640 medium with 10% fetal bovine serum (FBS) and 1% penicillin-streptomycin. MIA PaCa-2 and SW1573 were cultured in Dulbecco's modified Eagle's medium (DMEM)/F-12 medium with 10% FBS and 1% penicillin-streptomycin. MGH119 were cultured in DMEM with 10% FBS and 1% penicillin-streptomycin. 293FT cells were cultured in DMEM high-glucose medium with 10% FBS, 1% penicillin-streptomycin, 1% sodium pyruvate, 1% nonessential amino acids, and 1% GlutaMAX. All cell lines were purchased from the American Type Culture Collection or Duke University Cell Culture Facility except for MGH lines, which were obtained from A. Hata. Cell lines were authenticated using the Promega PowerPlex 18D kit. Drugs were purchased from APExBIO (osimertinib, gefitinib, SCH772984, ceritinib, quizartinib, PLX4720, AMG510, and lorlatinib), Cayman Chemical (olaparib), and SelleckChem (AZD0156, AZD1390, Q-VD-Oph, and cycloheximide).

Evolving drug-resistant cell lines and DTPs

To achieve drug resistance in vitro, PC9 cells were continuously cultured in increasing concentrations of drugs. Cells were first drugged at a dose about equal to their GI_{50} value (concentration for 50% of maximal inhibition of cell proliferation). The growth rate was monitored with weekly passaging, and the concentration of drug was increased once a stable growth rate was achieved. DTP cells were derived by treating drug-sensitive PC9 and MGH119 cells with the relevant drugs at concentrations greater than 100 times the established IC_{50} values (2 μM for gefitinib and 1 μM for osimertinib) for three successive rounds of culture, with each treatment lasting 72 hours. Viable cells remaining attached on the dish at the end of the third round of drug treatment were considered to be DTPs and were collected for use in subsequent analyses.

Short-term cell viability assays

For GI_{50} dose-response assays, cells were seeded into 96-well plates at a density of 4000 cells per well. Twenty-four hours after plating, cells were treated with vehicle [dimethyl sulfoxide (DMSO)] or a 10-fold serial dilution of drug. Each treatment condition was conducted in triplicate. Three days after the addition of drug, cell viability was quantified using CellTiter-Glo (CTG, Promega). The relative cell viability was determined by normalizing the raw luminescence values for each treatment condition to the DMSO-treated wells. For experiments involving two drugs, slight modifications were made. One drug was kept at a constant concentration across all wells, and a serial dilution of a second drug was added on top of the background drug. One set of triplicate wells was treated with DMSO only, and one set of triplicate wells was treated with background drug only. The relative cell viability was normalized to the luminescence of the background drug only. Dose-response curves were fit using GraphPad/Prism 7/8 software. Cell viabilities were reported as the percentage of cells (relative to DMSO-treated cells) that survived treatment at the indicated dose(s) of drug.

For bulk growth assays, cells were seeded in 10-cm plates at the following densities: PC9, 1×10^6; HCC827, 150,000; MOLM13, 1×10^6; PC9R, 500,000; GR4, 500,000; and WZR12, 500,000 cells. Twenty-four hours after plating, cells were treated with vehicle (DMSO) or the indicated dose of targeted therapy for 24 hours.

Each treatment was conducted in triplicate. After 24 hours of treatment, cells were harvested to obtain raw cell counts, reported as cell number. For DTPs, PC9 and MGH119 cells that remained after 9-day treatment with gefitinib or osimertinib were harvested and replated. DTP cells were treated with the appropriate EGFR inhibitor, AZD0156, or the combination of the two drugs for 4 days. Each treatment was conducted in triplicate. The percentage of viable cells (percentage of cells surviving treatment, normalized to EGFR inhibitor only–treated cells) is reported.

Annexin V staining

Annexin V staining was performed to determine the percentage of cells undergoing apoptosis. A total of 100,000 cells were plated in six-well plates and, 24 hours later, were treated with the indicated doses of vehicle (DMSO), targeted therapy, AZD0156, or the combination of drugs for 24 hours. Upon collection, cells were washed twice with phosphate-buffered saline (PBS), resuspended in 100 μl of 1× annexin V binding buffer (BD Biosciences) containing 5 μl of annexin V stain conjugated to APC (allophycocyanin) (BD Biosciences) and 5 μl of 7-aminoactinomycin D (7-AAD) (BD Biosciences). Phosphatidylserine externalization was measured using APC-conjugated annexin V, and 7-AAD was used as a viability probe. After a 15-min incubation at room temperature, the samples were analyzed using the flow cytometer BD FACSCanto II. The gating strategy was defined using untreated/unstained cells. Analysis of flow cytometry data was performed with FlowJo v10.

Cloning of constructs

CRISPR constructs were cloned following previously published methods (*33*) using previously characterized single guide RNAs (sgRNAs) (*34*). sgRNA inserts were synthesized by CustomArray in the form:

GGAAAGGACGAAACACCGXXXXXXXXXXXXXXXXXXXX-GTTTTAGAGCTAGAAATAGCAAGTTAAAATAAGGC.

"X" denotes unique 20-mer sgRNA sequence (see the 20-mer sequences below). The oligo pool was diluted 1:100 in water and amplified using New England Biolabs Phusion Hot Start Flex enzyme master mix and the primers Array F and Array R.

Array F: TAACTTGAAAGTATTTCGATTTCTTGGCTTTATAT-ATCTTGTGGAAAGGACGAAACACCG.

Array R: ACTTTTTCAAGTTGATAACGGACTAGCCTTATT TTAACTTGCTATTTCTAGCTCTAAAAC.

Polymerase chain reaction (PCR) protocol: 98°C/30 s, 18 × [98°C/10 s, 63°C/10 s, 72°C/15 s], and 72°C/3 min.

Inserts were cleaned with Axygen PCR cleanup beads (1.8×; Thermo Fisher Scientific) and resuspended in molecular biology grade water. LentiCRISPRv2 (Addgene ID 52961) was digested with Bsm BI (Thermo Fisher Scientific) for 2 hours at 37°C. The ~13-kb band was gel-extracted after size selection on 1% agarose gel. Using 100 ng of cut lentiCRISPRv2 and 40 ng of sgRNA oligos, a 20-ml Gibson assembly reaction was performed (30 min, 50°C). After Gibson assembly, 1 ml of the reaction was transformed into electrocompetent Lucigen cells, spread on LB-ampicillin plates, and incubated overnight. Single colonies were picked and grown overnight in liquid culture at 37°C. Plasmid extraction was performed using a Plasmid Miniprep kit (QIAGEN). DNA was used to make lentivirus as described below. shRNA glycerol stocks were obtained from the Duke Functional Genomics Core Facility. Glycerol stocks were streaked out on LB-ampicillin plates overnight. Subsequently, colonies were picked and grown overnight in liquid culture at 37°C. Plasmid extraction was performed using a Plasmid Miniprep kit (QIAGEN). DNA was used to make lentivirus as described below.

Lentivirus production and transduction

Human embryonic kidney 293T cells were grown in 10 cm to ~50% confluence. Per-plate transfection was performed using FuGENE 6 (Promega), 6.2 mg of psPAX2, 0.620 mg pVSVg, and 6.25 mg of CRISPR plasmid. After 30 min of incubation at room temperature, the mixture was added to the cells and incubated overnight. The next day, harvest media were added (DMEM and 30% FBS). After two consecutive 24-hour collections, the harvested virus was passed through a 0.45-μm filter. Transductions were performed by plating 200,000 cells in 2-ml RPMI 1640 media into six-well dishes. The following day, 0.5 ml of virus and 2 μg of polybrene were added to each well of the six-well plate. The cells were then centrifuged at 2500 rpm for 1 hour at 37°C and incubated overnight at 37°C. Twenty-four hours later, cells were selected with puromycin (2 μg/ml).

Immunoblotting

Immunoblotting was performed as previously described (*35*), with slight modification. Protein lysates were prepared with radioimmunoprecipitation assay lysis buffer supplemented with 1× protease inhibitor cocktail. Crude lysates were cleared using QIAshredder homogenizers (QIAGEN) and centrifuged at 13,000 rpm for 2 min at 4°C. Membranes were probed with the following primary antibodies: β-Actin [Cell Signaling Technology (CST), no. 4970], p-ATM (S1981) (Abcam, ab81292), ATM (CST no. 2873), γ-H2AX (p-histone H2A.X) (CST no. 9718), vinculin (CST, no. 4650), ATR (CST, no. 2790), p-Chk2 (T68) (CST, no. 2661), p-Chk1 (S317) (CST, no. 2344), caspase 9 (CST, no. 9502), caspase 3 (CST, no. 9662), cleaved caspase 3 (CST, no. 9661), caspase 7 (CST, no. 9492), BIM (CST, no. 2933), BAK (CST, no. 3814), BAX (CST, no. 2772), ICAD (Santa Cruz Biotechnology, sc17818), CAD (Santa Cruz Biotechnology, sc374067), p-EGFR (CST, no. 2234), T-EGFR (CST, no. 4267), p-ERK (CST, no. 4370), T-ERK (CST, no. 4695), p-MEK (CST, no. 9127), p-FLT3 (CST, no. 4577), EXO1 (Abcam, ab95068), BRCA1 (Santa Cruz Biotechnology, sc6954), BRCA2 (Santa Cruz Biotechnology, sc8326), RAD51B (Santa Cruz Biotechnology, sc377192), DNA polymerase iota (Abcam, ab157244), p-AKT S473 (CST, no. 9271), T-AKT (CST, no. 9272), Chk1 (CST, no. 2360), Chk2 (CST, no. 6334), H2AX (CST, no. 7631), and cytochrome c (CST, no. 11940). Primary antibodies were diluted 1:1000 in 5% bovine serum albumin (BSA) and incubated overnight (16 hours). After incubation with horseradish peroxidase–conjugated secondary antibody, blots were developed with SuperSignal West Pico PLUS Chemiluminescent Substrate (Thermo Fisher Scientific) or ECL Western Blotting Substrate (Thermo Fisher Scientific). For cell fractionation experiments, the cell fractionation kit (CST, no. 9038) was used according to the manufacturer's instructions. The Bradford method was additionally used to normalize protein concentrations of all samples in these experiments, including the cytoplasmic- and membrane-bound fractions.

TTP assay

To evaluate the relative ability of treatments to delay the reemergence of logarithmic cell growth in vitro (resistance), cells were plated in triplicate in 6-cm plates at 100,000 cells per plate in normal growth media. After 24 hours, the growth media were replaced

with the indicated treatment. At the time points indicated, the cells were lifted with 0.25% trypsin (Life Technologies) and counted using a Z2 coulter particle count and size analyzer (Beckman Coulter, Pasadena, CA). All cells up to 100,000 were centrifuged at 1200 rpm for 5 min, resuspended in 3 ml of media, and then plated in a 6-cm plate with fresh treatment. This procedure was repeated weekly for 4 to 12 weeks, depending on the kinetics of resistance. Weekly growth rates (μ) were calculated from the number of cells plated the previous week (N_0) and the number counted the current week (N) according to the formula $\ln N = \ln N_0 + \mu^* t$; where t is elapsed time. These growth rates were then used to project the total virtual cell number.

Neutral comet assay

Trevigen Kit was used according to the neutral comet assay protocol conditions (Trevigen, 4250-050-K). DMSO (vehicle) was used as a negative control, and 10-Gy irradiation immediately before harvest was used as a positive control. All vehicle and drug treatments were performed for 24 hours. Cells were imaged on the Live Cell Station 1: Zeiss Axio Observer inverted microscope using the following specifications: ×10 magnification on the green fluorescent protein (GFP) (488-nm) channel and 450-ms exposure time. Comet analysis was done using CellProfiler. Pipeline was optimized using negative-control and positive-control images only. Comets with no comet head (debris) were thrown out. For quantification, extent tail moment was calculated as follows: extent tail moment = tail DNA% × length of tail. Results show are the mean extent tail moment and the SEM obtained from several hundred images per treatment condition.

Immunofluorescence

Immunofluorescence assay to detect Rad51 foci was performed as previously described (*36*, *37*), with minor modifications. Cell lines were plated on glass coverslips and, the following day, were treated with 100 nM gefitinib, 1.5 μM AZD0156, and/or Q-VD-OPh for 24 hours. Cells were fixed with 3% paraformaldehyde (20 min at room temperature). The cells were then washed 4× 15 min in PBS-T (PBS containing 0.15% BSA and 0.1% Triton X-100). Slides were then incubated with anti-Rad51 (200 ng/ml; Santa Cruz Biotechnology) overnight, washed in PBS-T, and incubated with Alexa Fluor 488–conjugated goat anti-rabbit immunoglobulin G (CST) at 1:1000 dilution for 1 hour. Last, the cells were washed three times with PBS-T and mounted using Prolong Gold Antifade reagent with 4′,6-diamidino-2-phenylindole (Life Technologies). The slides were then imaged using a Leica SP5 inverted confocal microscope with a ×40 oil objective. For all representative images in the manuscript, experiments were conducted at least twice and had no repeatability issues. Percentage of $Rad51^+$ cells was calculated by visual scoring of cells in the images obtained, with only cells having five or greater GFP-staining foci being termed as $Rad51^+$. Fifty to 100 cells were scored/treatment condition.

Immunohistochemistry

All patient tumor samples analyzed were obtained under Institutional Review Board–approved protocols with informed consent obtained from each patient under the guidance of the University of California, San Francisco (UCSF). All relevant ethical regulations were followed. The mutational status of *EGFR* or other known drivers of resistance was determined using FoundationOne (Foundation Medicine) or internal UCSF molecular pathology evaluation (UCSF 500). Tissues were fixed in 10% formalin overnight and embedded in paraffin. Tissue sections of patient-derived xenograft (PDX) and patient samples were sectioned on slides with a thickness of 4 μm. After IHC preparation of slides and staining via p-ATM antibody, slides were imaged and analyzed for staining intensity. Images were taken at ×20 magnification using the Olympus BX46 light microscope. The analysis was based on the staining intensity and percentage of cells staining positive for p-ATM. The staining area was scored using the following scale: 0, 0 to 10%; 1, 10 to 20% of tissue stained positive; 2, 20 to 40% stained positive; 3, 40 to 70% stained positive; and 4, >70% positive cells. Average IHC scores were generated from visualization of three different areas of the slide for each sample.

In vivo studies

All animal procedures and studies were approved by the Institutional Animal Care and Use Committee at Duke University. NSCLC cell lines (PC9, H1975, or MGH134) were evaluated by IMPACT testing before their use in vivo. About 0.5 to 1×10^6 cells were suspended in a PBS and Matrigel solution (PBS:Matrigel = 1:1), and 100 μl of cell suspension was subcutaneously injected into the flank of ~6- to 8-week-old female nude mice. Tumor size was measured three times weekly with calipers, and tumor volume was calculated by the formula: $V = L \times W^2 \times 0.52$ (L = longest diameter and W = shortest diameter). When tumor volume reached ~100 to 200 mm^3, mice were randomized into treatment groups, with each group having five to six mice. AZD0156 and osimertinib were purchased from Selleck-Chem (USA). AZD0156 was resuspended in ORA-Plus suspension (clinical grade; purchased from Duke Pharmacy Stock Room), and osimertinib was dissolved in a 10% DMSO, 30% polyethylene glycol, molecular weight 400, and 60% H_2O solution. All drugs were administered orally with 100 μl of drug suspension/dose per mouse. AZD0156 was administrated at 50 mg/kg daily, and osimertinib was administrated at 5 mg/kg daily. All mice were dosed Monday to Friday (5 days per week). Tumor size was monitored two to three times per week until the end point when tumors reached ~1000 mm^3 or tumors were ulcerated.

Statistical analyses

All results are shown as means ± SEM, unless otherwise shown. P values were determined using unpaired, two-tailed Student's t tests, Mann-Whitney test, or, for grouped analyses, one-way analysis of variance (ANOVA) with Tukey's post hoc test; $P < 0.05$ was considered significant. Unless otherwise noted, all experiments were performed a minimum of three times, and measurements were taken from distinct biological replicate samples.

SUPPLEMENTARY MATERIALS

www.science.org/doi/10.1126/scitranslmed.abc7480
Figs. S1 to S4
Tables S1 to S3
Data file S1
MDAR Reproducibility Checklist

View/request a protocol for this paper from *Bio-protocol*.

REFERENCES AND NOTES

1. D. A. Haber, N. S. Gray, J. Baselga, The evolving war on cancer. *Cell* **145**, 19–24 (2011).
2. V. V. Padma, An overview of targeted cancer therapy. *Biomedicine* **5**, 19 (2015).
3. Y. K. Chae, A. P. Pan, A. A. Davis, S. P. Patel, B. A. Carneiro, R. Kurzrock, F. J. Giles, Path toward precision oncology: Review of targeted therapy studies and tools to aid

in defining "actionability" of a molecular lesion and patient management support. *Mol. Cancer Ther.* **16**, 2645–2655 (2017).
4. N. Amirouchene-Angelozzi, C. Swanton, A. Bardelli, Tumor evolution as a therapeutic target. *Cancer Discov.* **7**, 805–817 (2017).
5. C. E. McCoach, T. G. Bivona, Engineering multidimensional evolutionary forces to combat cancer. *Cancer Discov.* **9**, 587–604 (2019).
6. N. Chatterjee, T. G. Bivona, Polytherapy and targeted cancer drug resistance. *Trends Cancer* **5**, 170–182 (2019).
7. T. G. Bivona, R. C. Doebele, A framework for understanding and targeting residual disease in oncogene-driven solid cancers. *Nat. Med.* **22**, 472–478 (2016).
8. C. Sun, Y. Fang, J. Yin, J. Chen, Z. Ju, D. Zhang, X. Chen, C. P. Vellano, K. J. Jeong, P. K. Ng, A. K. B. Eterovic, N. H. Bhola, Y. Lu, S. N. Westin, J. R. Grandis, S. Y. Lin, K. L. Scott, G. Peng, J. Brugge, G. B. Mills, Rational combination therapy with PARP and MEK inhibitors capitalizes on therapeutic liabilities in *RAS* mutant cancers. *Sci. Transl. Med.* **9**, eaal5148 (2017).
9. O. Maertens, R. Kuzmickas, H. E. Manchester, C. E. Emerson, A. G. Gavin, C. J. Guild, T. C. Wong, T. De Raedt, C. Bowman-Colin, E. Hatchi, L. A. Garraway, K. T. Flaherty, S. Pathania, S. J. Elledge, K. Cichowski, MAPK pathway suppression unmasks latent DNA repair defects and confers a chemical synthetic vulnerability in *BRAF*-, *NRAS*-, and *NF1*-mutant melanomas. *Cancer Discov.* **9**, 526–545 (2019).
10. M. Russo, G. Crisafulli, A. Sogari, N. M. Reilly, S. Arena, S. Lamba, A. Bartolini, V. Amodio, A. Magri, L. Novara, I. Sarotto, Z. D. Nagel, C. G. Piett, A. Amatu, A. Sartore-Bianchi, S. Siena, A. Bertotti, L. Trusolino, M. Corigliano, M. Gherardi, M. C. Lagomarsino, F. Di Nicolantonio, A. Bardelli, Adaptive mutability of colorectal cancers in response to targeted therapies. *Science* **366**, 1473–1480 (2019).
11. Y. H. Ibrahim, C. Garcia-Garcia, V. Serra, L. He, K. Torres-Lockhart, A. Prat, P. Anton, P. Cozar, M. Guzman, J. Grueso, O. Rodriguez, M. T. Calvo, C. Aura, O. Diez, I. T. Rubio, J. Perez, J. Rodon, J. Cortes, L. W. Ellisen, M. Scaltriti, J. Baselga, PI3K inhibition impairs BRCA1/2 expression and sensitizes BRCA-proficient triple-negative breast cancer to PARP inhibition. *Cancer Discov.* **2**, 1036–1047 (2012).
12. A. Juvekar, L. N. Burga, H. Hu, E. P. Lunsford, Y. H. Ibrahim, J. Balmana, A. Rajendran, A. Papa, K. Spencer, C. A. Lyssiotis, C. Nardella, P. P. Pandolfi, J. Baselga, R. Scully, J. M. Asara, L. C. Cantley, G. M. Wulf, Combining a PI3K inhibitor with a PARP inhibitor provides an effective therapy for BRCA1-related breast cancer. *Cancer Discov.* **2**, 1048–1063 (2012).
13. P. A. Konstantinopoulos, W. T. Barry, M. Birrer, S. N. Westin, K. A. Cadoo, G. I. Shapiro, E. L. Mayer, R. E. O'Cearbhaill, R. L. Coleman, B. Kochupurakkal, C. Whalen, J. Curtis, S. Farooq, W. Luo, J. Eismann, M. K. Buss, C. Aghajanian, G. B. Mills, S. Palakurthi, P. Kirschmeier, J. Liu, L. C. Cantley, S. H. Kaufmann, E. M. Swisher, A. D. D'Andrea, E. Winer, G. M. Wulf, U. A. Matulonis, Olaparib and α-specific PI3K inhibitor alpelisib for patients with epithelial ovarian cancer: A dose-escalation and dose-expansion phase 1b trial. *Lancet Oncol.* **20**, 570–580 (2019).
14. E. M. Tricker, C. Xu, S. Uddin, M. Capelletti, D. Ercan, A. Ogino, C. A. Pratilas, N. Rosen, N. S. Gray, K. K. Wong, P. A. Janne, Combined EGFR/MEK inhibition prevents the emergence of resistance in EGFR-mutant lung cancer. *Cancer Discov.* **5**, 960–971 (2015).
15. X. Liu, F. Li, Q. Huang, Z. Zhang, L. Zhou, Y. Deng, M. Zhou, D. E. Fleenor, H. Wang, M. B. Kastan, C. Y. Li, Self-inflicted DNA double-strand breaks sustain tumorigenicity and stemness of cancer cells. *Cell Res.* **27**, 764–783 (2017).
16. A. N. Hata, J. A. Engelman, A. C. Faber, The BCL2 family: Key mediators of the apoptotic response to targeted anticancer therapeutics. *Cancer Discov.* **5**, 475–487 (2015).
17. K. A. Sarosiek, X. Chi, J. A. Bachman, J. J. Sims, J. Montero, L. Patel, A. Flanagan, D. W. Andrews, P. Sorger, A. Letai, BID preferentially activates BAK while BIM preferentially activates BAX, affecting chemotherapy response. *Mol. Cell* **51**, 751–765 (2013).
18. T. C. Chou, Drug combination studies and their synergy quantification using the Chou-Talalay method. *Cancer Res.* **70**, 440–446 (2010).
19. S. V. Sharma, D. Y. Lee, B. Li, M. P. Quinlan, F. Takahashi, S. Maheswaran, U. McDermott, N. Azizian, L. Zou, M. A. Fischbach, K. K. Wong, K. Brandstetter, B. Wittner, S. Ramaswamy, M. Classon, J. Settleman, A chromatin-mediated reversible drug-tolerant state in cancer cell subpopulations. *Cell* **141**, 69–80 (2010).
20. S. Misale, I. Bozic, J. Tong, A. Peraza-Penton, A. Lallo, F. Baldi, K. H. Lin, M. Truini, L. Trusolino, A. Bertotti, F. Di Nicolantonio, M. A. Nowak, L. Zhang, K. C. Wood, A. Bardelli, Vertical suppression of the EGFR pathway prevents onset of resistance in colorectal cancers. *Nat. Commun.* **6**, 8305 (2015).
21. A. S. Crystal, A. T. Shaw, L. V. Sequist, L. Friboulet, M. J. Niederst, E. L. Lockerman, R. L. Frias, J. F. Gainor, A. Amzallag, P. Greninger, D. Lee, A. Kalsy, M. Gomez-Caraballo, L. Elamine, E. Howe, W. Hur, E. Lifshits, H. E. Robinson, R. Katayama, A. C. Faber, M. M. Awad, S. Ramaswamy, M. Mino-Kenudson, A. J. Iafrate, C. H. Benes, J. A. Engelman, Patient-derived models of acquired resistance can identify effective drug combinations for cancer. *Science* **346**, 1480–1486 (2014).
22. A. N. Hata, M. J. Niederst, H. L. Archibald, M. Gomez-Caraballo, F. M. Siddiqui, H. E. Mulvey, Y. E. Maruvka, F. Ji, H. E. Bhang, V. Krishnamurthy Radhakrishna, G. Siravegna, H. Hu, S. Raoof, E. Lockerman, A. Kalsy, D. Lee, C. L. Keating, D. A. Ruddy, L. J. Damon, A. S. Crystal, C. Costa, Z. Piotrowska, A. Bardelli, A. J. Iafrate, R. I. Sadreyev, F. Stegmeier, G. Getz, L. V. Sequist, A. C. Faber, J. A. Engelman, Tumor cells can follow distinct evolutionary paths to become resistant to epidermal growth factor receptor inhibition. *Nat. Med.* **22**, 262–269 (2016).
23. H. A. Yu, M. E. Arcila, N. Rekhtman, C. S. Sima, M. F. Zakowski, W. Pao, M. G. Kris, V. A. Miller, M. Ladanyi, G. J. Riely, Analysis of tumor specimens at the time of acquired resistance to EGFR-TKI therapy in 155 patients with EGFR-mutant lung cancers. *Clin. Cancer Res.* **19**, 2240–2247 (2013).
24. B. Zhao, J. C. Sedlak, R. Srinivas, P. Creixell, J. R. Pritchard, B. Tidor, D. A. Lauffenburger, M. T. Hemann, Exploiting temporal collateral sensitivity in tumor clonal evolution. *Cell* **165**, 234–246 (2016).
25. L. Marcar, K. Bardhan, L. Gheorghiu, P. Dinkelborg, H. Pfaffle, Q. Liu, M. Wang, Z. Piotrowska, L. V. Sequist, K. Borgmann, J. E. Settleman, J. A. Engelman, A. N. Hata, H. Willers, Acquired resistance of EGFR-mutated lung cancer to tyrosine kinase inhibitor treatment promotes PARP inhibitor sensitivity. *Cell Rep.* **27**, 3422–3432.e4 (2019).
26. L. Wang, R. Leite de Oliveira, S. Huijberts, E. Bosdriesz, N. Pencheva, D. Brunen, A. Bosma, J. Y. Song, J. Zevenhoven, G. T. Los-de Vries, H. Horlings, B. Nuijen, J. H. Beijnen, J. H. M. Schellens, R. Bernards, An acquired vulnerability of drug-resistant melanoma with therapeutic potential. *Cell* **173**, 1413–1425.e14 (2018).
27. K. R. Singleton, L. Crawford, E. Tsui, H. E. Manchester, O. Maertens, X. Liu, M. V. Liberti, A. N. Magpusao, E. M. Stein, J. P. Tingley, D. T. Frederick, G. M. Boland, K. T. Flaherty, S. J. McCall, C. Krepler, K. Sproesser, M. Herlyn, D. J. Adams, J. W. Locasale, K. Cichowski, S. Mukherjee, K. C. Wood, Melanoma therapeutic strategies that select against resistance by exploiting MYC-driven evolutionary convergence. *Cell Rep.* **21**, 2796–2812 (2017).
28. M. J. Hangauer, V. S. Viswanathan, M. J. Ryan, D. Bole, J. K. Eaton, A. Matov, J. Galeas, H. D. Dhruv, M. E. Berens, S. L. Schreiber, F. McCormick, M. T. McManus, Drug-tolerant persister cancer cells are vulnerable to GPX4 inhibition. *Nature* **551**, 247–250 (2017).
29. V. S. Viswanathan, M. J. Ryan, H. D. Dhruv, S. Gill, O. M. Eichhoff, B. Seashore-Ludlow, S. D. Kaffenberger, J. K. Eaton, K. Shimada, A. J. Aguirre, S. R. Viswanathan, S. Chattopadhyay, P. Tamayo, W. S. Yang, M. G. Rees, S. Chen, Z. V. Boskovic, S. Javaid, C. Huang, X. Wu, Y. Y. Tseng, E. M. Roider, D. Gao, J. M. Cleary, B. M. Wolpin, J. P. Mesirov, D. A. Haber, J. A. Engelman, J. S. Boehm, J. D. Kotz, C. S. Hon, Y. Chen, W. C. Hahn, M. P. Levesque, J. G. Doench, M. E. Berens, A. F. Shamji, P. A. Clemons, B. R. Stockwell, S. L. Schreiber, Dependency of a therapy-resistant state of cancer cells on a lipid peroxidase pathway. *Nature* **547**, 453–457 (2017).
30. K. H. Lin, J. C. Rutter, A. Xie, E. Winn, B. Pardieu, R. Dal Bello, R. Itzykson, Y. R. Ahn, Z. Dai, R. T. Sobhan, G. R. Anderson, K. R. Singleton, A. E. Decker, P. S. Winter, J. W. Locasale, L. Crawford, A. Puissant, K. C. Wood, Using antagonistic pleiotropy to design a chemotherapy-induced evolutionary trap to target drug resistance in cancer. *Nat. Genet.* **52**, 408–417 (2020).
31. O. L. Kantidze, A. K. Velichko, A. V. Luzhin, N. V. Petrova, S. V. Razin, Synthetically lethal interactions of ATM, ATR, and DNA-PKcs. *Trends Cancer* **4**, 755–768 (2018).
32. S. T. Durant, L. Zheng, Y. Wang, K. Chen, L. Zhang, T. Zhang, Z. Yang, L. Riches, A. G. Trinidad, J. H. L. Fok, T. Hunt, K. G. Pike, J. Wilson, A. Smith, N. Colclough, V. P. Reddy, A. Sykes, A. Janefeldt, P. Johnstrom, K. Varnas, A. Takano, S. Ling, J. Orme, J. Stott, C. Roberts, I. Barrett, G. Jones, M. Roudier, A. Pierce, J. Allen, J. Kahn, A. Sule, J. Karlin, A. Cronin, M. Chapman, K. Valerie, R. Illingworth, M. Pass, The brain-penetrant clinical ATM inhibitor AZD1390 radiosensitizes and improves survival of preclinical brain tumor models. *Sci. Adv.* **4**, eaat1719 (2018).
33. O. Shalem, N. E. Sanjana, E. Hartenian, X. Shi, D. A. Scott, T. S. Mikkelsen, D. Heckl, B. L. Ebert, D. E. Root, J. G. Doench, F. Zhang, Genome-scale CRISPR-Cas9 knockout screening in human cells. *Science* **343**, 84–87 (2014).
34. T. Wang, J. J. Wei, D. M. Sabatini, E. S. Lander, Genetic screens in human cells using the CRISPR-Cas9 system. *Science* **343**, 80–84 (2014).
35. M. Ali, E. Kaltenbrun, G. R. Anderson, S. J. Stephens, S. Arena, A. Bardelli, C. M. Counter, K. C. Wood, Codon bias imposes a targetable limitation on KRAS-driven therapeutic resistance. *Nat. Commun.* **8**, 15617 (2017).
36. R. Montano, R. Thompson, I. Chung, H. Hou, N. Khan, A. Eastman, Sensitization of human cancer cells to gemcitabine by the Chk1 inhibitor MK-8776: Cell cycle perturbation and impact of administration schedule in vitro and in vivo. *BMC Cancer* **13**, 604 (2013).
37. G. R. Anderson, S. E. Wardell, M. Cakir, C. Yip, Y. R. Ahn, M. Ali, A. P. Yllanes, C. A. Chao, D. P. McDonnell, K. C. Wood, Dysregulation of mitochondrial dynamics proteins are a targetable feature of human tumors. *Nat. Commun.* **9**, 1677 (2018).

Acknowledgments: We thank the members of the K.C.W., T.G.B., C.E.M., C.M.B., A.N.H., and H.A.Y. laboratories for helpful discussions and scientific input. We also thank S. Floyd and C.-Y. Li (Duke Pharmacology and Cancer Biology) for providing helpful commentary on this work. **Funding:** This work was supported by Duke University School of Medicine start-up funds and support from the Duke Cancer Institute (to K.C.W.), NIH awards (R01CA207083 to

K.C.W.; F30CA220847 to M.A.; F32CA206234 to R.S.S.; and R01CA231300, U54CA224081, R01CA204302, R01CA211052, R01CA169338, and U01CA217882 to T.G.B.), the Duke Medical Scientist Training Program (T32 GM007171 to M.A.), the Pew-Stewart Foundation (to T.G.B.), and the Agency for Science, Technology and Research, Singapore (NSS-PhD to H.X.A.). **Author contributions:** M.A., R.S.S., O.M.L., and K.C.W. conceptualized the project. M.A., M.L., C.F.B., A.N.H., and K.C.W. were responsible for methodology. In vitro mechanistic and validation studies were performed by M.A., M.L., H.X.A., R.S.S., H.M.H., and C.F.B. In vivo mechanistic and validation studies were performed by M.A., M.L., C.E.E., and D.L.K. Tumor specimens were cataloged and analyzed by M.A., C.G., C.M.B., C.E.M., T.G.B., and K.C.W. Tumor genome sequences and associated survival analyses were performed by M.A., C.J.F., H.A.Y., and K.C.W. Data were curated by M.A. and K.C.W. The original draft was written by M.A. and K.C.W. All authors reviewed and edited the paper. M.A. was responsible for visualization. K.C.W. supervised the project. Funding was acquired by M.A., H.X.A., R.S.S., T.G.B., and K.C.W. **Competing interests:** K.C.W. is a cofounder and consultant for Element Genomics, Tavros Therapeutics, and Celldom. A.N.H. has served as a consultant for Nuvalent Inc. and receives research funding from Pfizer, Relay Therapeutics, Roche/Genentech, Eli Lilly and Company, Blueprint Medicines, and Amgen. T.G.B. is an advisor to Novartis, AstraZeneca, Revolution Medicines, Array/Pfizer, SpringWorks, Strategia Therapeutics, Relay Therapeutics, Jazz Pharmaceuticals, Rain Therapeutics, and EcoR1 and receives research funding from Novartis, Revolution Medicines, and Strategia Therapeutics. C.M.B. has performed consulting work for Revolution Medicines, Blueprint Medicines, Amgen, Bayer, and Foundation Medicine. H.A.Y. has performed consulting work for Daiichi, Janssen Pharmaceuticals, Blueprint Medicines, and AstraZeneca. C.G. is a scientific advisor for SafineAI LLC. C.E.M. is an employee of Genentech Inc.; has performed unpaid consulting for Eli Lilly and Company and Loxo; has received honoraria from Genentech, AstraZeneca, Takeda, Novartis, and GuardantHealth; and receives/received research funding from Novartis and Revolution Medicines. **Data and materials availability:** All data associated with this study are present in the paper or the Supplementary Materials.

Submitted 11 May 2020
Resubmitted 10 October 2021
Accepted 11 March 2022
Published 30 March 2022
10.1126/scitranslmed.abc7480

Science Translational Medicine

Small-molecule targeted therapies induce dependence on DNA double-strand break repair in residual tumor cells

Moiez AliMin LuHazel Xiaohui AngRyan S. SoderquistChristine E. EylerHaley M. HutchinsonCarolyn GlassChristopher F. BassilOmar M. LopezD. Lucas KerrChristina J. FalconHelena A. YuAaron N. HataCollin M. BlakelyCaroline E. McCoachTrever G. BivonaKris C. Wood

Sci. Transl. Med., 14 (638), eabc7480. • DOI: 10.1126/scitranslmed.abc7480

Ablating residual cells with ATM inhibitors

Although oncogene-targeted therapy offers a personalized approach to cancer treatment, most patients with advanced disease quickly develop resistance. Ali *et al*. show here that these therapies induce DNA double-stranded breaks reliant on repair by ataxia-telangiectasia mutated (ATM), representing a potential mechanism to overcome this resistance. For example, they demonstrated that combined ATM and epidermal growth factor receptor (EGFR) inhibitors can eradicate non–small cell lung cancer cells in mouse xenografts. Several ATM kinase inhibitors are already in clinical development, which represents an opportunity for combination with oncogene-targeted therapies to overcome resistance in a variety of cancer types.